

Copy
RM L53H25

NACA RM L53H25

NACA

TECH LIBRARY KAFB, NM

0144267



RESEARCH MEMORANDUM

7462

INVESTIGATION AT MACH NUMBERS OF 1.62, 1.93, AND 2.41 OF
THE EFFECT OF OSCILLATION AMPLITUDE ON THE DAMPING
IN PITCH OF DELTA-WING-BODY COMBINATIONS

By Arthur Henderson, Jr.

Langley Aeronautical Laboratory
Langley Field, Va.

**NATIONAL ADVISORY COMMITTEE
FOR AERONAUTICS**

WASHINGTON

October 26, 1953

Classification cancelled (or changed to *CONFIDENTIAL*)

By authority of *W.H.S.A. TEC-4 PWD Admin Management*
(OFFICER AUTHORITY TO DO THIS)

By *W.H.S.A.* *26 Aug 57*

TYPE OF OFFICE *(LISTING CHANGES)* *R.G.B.*

Branch Office
DATE



0144267

NATIONAL ADVISORY COMMITTEE FOR AERONAUTICS

RESEARCH MEMORANDUM

INVESTIGATION AT MACH NUMBERS OF 1.62, 1.93, AND 2.41 OF
THE EFFECT OF OSCILLATION AMPLITUDE ON THE DAMPING
IN PITCH OF DELTA-WING-BODY COMBINATIONS

By Arthur Henderson, Jr.

SUMMARY

In order to assess the validity of the linear theory, which accounts for neither viscous nor amplitude effects, tests were made of four delta-wing and body combinations at Mach numbers of 1.62, 1.93, and 2.41, and covering a Reynolds number range of 0.44×10^6 to 1.69×10^6 to determine the effect of oscillation amplitude on the damping in pitch.

The body in each case was the same; the wings had 25° , 30° , 35° , and 45° semiapex angles and were flat plates with beveled edges.

The results show that in some cases there is a small variation of damping with amplitude which is usually one of increasing damping with decreasing amplitude. A comparison of theory with experiment indicates that, in general, the damping in pitch of delta-wing-body combinations may be satisfactorily approximated by theory.

INTRODUCTION

The theoretical prediction of the damping in pitch of wings is limited by the restrictions inherent in the linear theory which, by its nature, is unable to show any effect of viscosity or variation of the damping-in-pitch parameter $C_{m_q} + C_{m_d}$ with amplitude. The responsibility of determining where, if at all, the existing theory is applicable, lies with the experimenter. There are two basic experimental techniques available by which the damping-in-pitch parameter can be determined, by the free-oscillation technique and the forced-oscillation technique. References 1 and 2 present data obtained from free oscillations at both subsonic and supersonic speeds and reference 3 presents data obtained from forced oscillations at subsonic speeds. Reference 3 shows the effect of oscillation amplitude and frequency on damping in pitch.

The present paper presents the effect of oscillation amplitude on damping in pitch at three supersonic Mach numbers, 1.62, 1.93, and 2.41, for three wing-body combinations. A fourth configuration, the data for which were not reducible, is discussed.

SYMBOLS

c	root chord (including part of wing submerged in the body)
\bar{c}	mean aerodynamic chord, $2/3c$
c_o	distance from wing apex to point of rotation
D	damping moment per time rate of change of angle of attack
I	moment of inertia
K	restoring moment per unit angle of attack
l	distance from model center of gravity to point of rotation
M	Mach number or pitching moment
m	mass of model
q	angular velocity of pitch
R	Reynolds number
S	wing area (including part of wing submerged in the body)
t	time
v	velocity
α	angle of attack
α_o	amplitude
$\beta = \sqrt{M^2 - 1}$	
ϵ	wing semiapex angle
ρ	density
ω	frequency, radians/sec

$\bar{\omega}$ reduced frequency, $\omega\bar{c}/2V$

C_m pitching-moment coefficient, $M/\frac{1}{2}\rho V^2 S \bar{c}$

$$C_{m\alpha} = \frac{\partial C_m}{\partial \alpha}$$

$$C_{mq} = \frac{\partial C_m}{\partial \frac{q\bar{c}}{2V}}$$

$$C_{m\dot{\alpha}} = \frac{\partial C_m}{\partial \frac{\dot{\alpha}\bar{c}}{2V}}$$

Subscripts:

i wind off

a wind on minus wind off

cg center of gravity

A dot above a symbol denotes differentiation with respect to time.

APPARATUS AND TESTS

Wind Tunnel

All tests were made in the Langley 9-inch supersonic tunnel. The tunnel is of the continuous-operation complete-return type in which the stream pressure, temperature, and humidity can be controlled. Within the stagnation chamber ahead of the first minimum are located 11 fine-mesh turbulence-damping screens. The Mach number is varied by interchanging nozzle blocks which form test sections approximately 9 inches square. The air was dried sufficiently for each test so that the condensation effects in the test section were negligible.

Models

The models tested in the present investigation consisted of four delta-wing and slender-body combinations. The body in each case was the

same (fineness ratio, 11.3) and consisted of a parabolic nose section, a circular cylindrical section along the wing-body juncture, and a boattailed afterbody. The wings had semiapex angles of 25° , 30° , 35° , and 45° , and the ratios of body diameter to wing span were 0.147, 0.132, 0.120, and 0.100, respectively.

Figure 1 presents the models tested. Figure 1(a) gives the body dimensions and shows the relative wing positions and figure 1(b) is a photograph of the component parts. The models were so constructed that each configuration consisted of four parts: (1) a nose and hollow barrel with internally threaded end; (2) an internally and externally threaded collar which screwed into the hollow-barrel end; (3) a sleeve which slid over the hollow barrel and to which were soldered the wings to be tested and two smaller flat-plate yaw-stabilizing fins; and (4) a hollow shaft the threaded end of which screwed into the internal threads of the collar and the flat-head end of which was beveled to fair in with the rear of the boattailed sleeve.

Model Support System

In figure 2 is shown a model mounted in a mock-up of the test section. The support system consisted of a crossed flexural pivot assembly within the model and a 1/16-inch-diameter piano wire. One base of the flexural pivot (see fig. 3) made a push fit with the hollow-body barrel to which it was pinned when in place. The other base of the pivot was smaller in diameter than the inside diameter of the barrel, allowing this end to oscillate with respect to the body. The piano wire was fastened securely to one tunnel wall, passed through the free end of the pivot by means of oblong slots in the sides of the body, and was secured by a yoke with a screw adjustment to a strain-gage beam on the outside of the other wall of the tunnel. (See fig. 2.) The screw adjustment and strain-gage beam allowed the tension on the wire to be held constant at approximately 250 pounds throughout all tests. Two set screws in the flat end of the free flexural pivot base clamped the base to the wire so the model was free to oscillate with respect to the wire.

Mounted on the side wall of the tunnel behind the model was a spring-loaded mechanism through which the positioning of a guided wire could be controlled. The model was given its initial displacement by inserting the end of the guided wire into a small hole in the base of the model and retracting the wire any desired distance. Triggering the mechanism successively released the wire from the body and removed the guide from the wake of the body. These two actions were practically simultaneous.

Recording of Data

A line source of light from a GE-853 bulb was focused on a 1/16-inch-diameter silvered mirror which was imbedded in the surface of the body

directly over the point of rotation. The line from the light source was then reflected onto a moving film strip through a horizontal slit in a 20-foot high-speed film drum. Since the film speed was not constant, the pulses from a GE-AR8 argon timing light were recorded on the film strip along with the model oscillation record. A typical oscillation record is shown in figure 4.

Displacements on the film strip were calibrated with measured angular displacements of the model.

EXPERIMENT

Scope of Tests

The present investigation was conducted at Mach numbers of 1.62, 1.93, and 2.41 and covered a Reynolds number range of 0.44×10^6 to 1.69×10^6 based on the mean aerodynamic chord of the wing (including the portion submerged in the body).

Every model was tested at two or more Reynolds numbers at each Mach number. In order to check repeatability, two or more complete sets of data were taken and all are presented. All models were oscillated about 0° angle of attack.

Reduction of Data

The single degree of freedom, free-oscillation technique was used to determine the damping-in-pitch characteristics of the models of the present investigation. With viscous damping and a nonvariable spring constant, this motion is described by the following equation:

$$I\ddot{\alpha} + D\dot{\alpha} + K\alpha = 0 \quad (1)$$

The solution to equation (1) is

$$\alpha = (\alpha_0)_{t=0} e^{-\frac{D}{2I}t} \left(\cos \omega t + \frac{D}{2I\omega} \sin \omega t \right) \quad (2)$$

where

$$\omega = \sqrt{\frac{K}{I} - \left(\frac{D}{2I} \right)^2}$$

~~CONFIDENTIAL~~

NACA RM L53H25

The expression which represents the envelope of the oscillations is

$$\alpha = \alpha_0 e^{-\frac{D}{2I}t} \quad (3)$$

In the ideal case the term $\frac{D}{2I}$ (which is a measure of the damping) is determined by plotting α of the envelope against t on a semilog scale. This plot is a straight line, the slope of which is $-\frac{D}{2I}$.

In the present investigation, since the oscillation-record envelopes could not be represented by equation (3) throughout the whole oscillation, it was assumed that the oscillation record could be represented by a series of segments, each segment of which could be represented by equation (3) with the appropriate value of $\frac{D}{2I}$. These segments may be made as small as desired. Differentiating equation (3) with respect to time and letting time approach zero for each segment gives

$$\frac{1}{\alpha_0} \left(\frac{d\alpha}{dt} \right)_{t \rightarrow 0} = -\frac{D}{2I} \quad (4)$$

Thus $-\frac{D}{2I}$ is the reciprocal of the number of time units lying between the time ordinate of a point on the envelope and the intercept on the $\alpha = 0$ axis of the tangent to that point. The term $\frac{D}{2I}$ is then determined as a function of amplitude.

To make use of the previously mentioned method of reducing the data, the following procedure was employed. The peaks of the oscillation record were read on a telereader and plotted. The amplitudes were plotted to 5 times actual size and the time scale was adjusted to facilitate plotting. Curves were then faired through the upper and lower peaks and the $\alpha = 0$ line was determined. At arbitrarily selected points along the upper curve, tangents were drawn to the curve and extended until they intersected the $\alpha = 0$ line. The same thing was done at corresponding points on the lower curve. The reciprocal of the number of time units between the time ordinate on the curve and the intercept on the $\alpha = 0$ line was taken to be $\frac{D}{2I}$ for the point.

In the present paper, both the damping-in-pitch parameter $C_{mq} + C_{m\dot{q}}$ and the pitching-moment derivative $C_{m\alpha}$ are found. Inasmuch as, with the wind on, equation (1) is

~~CONFIDENTIAL~~

$$I\ddot{\alpha} + (D_a + D_i)\dot{\alpha} + (K_a + K_i)\alpha = 0 \quad (5)$$

it is necessary to determine I , D_i , and K_i , in order to be able to separate the aerodynamic terms from the total result, and to evaluate D from $\frac{D}{2I}$.

The moment of inertia at the center of gravity I_{cg} was measured according to the bifilar pendulum equation

$$I_{cg} = \frac{Wd^2r(1-r)}{\omega^2 s} \quad (6)$$

where

W weight of configuration

ω frequency in radians per second

d , s , r symbols defined in figure 5

The value of I for the test was then determined by the equation

$$I = I_{cg} + ml^2$$

Equation (6) is derived on the assumption of small angles; that is, sines and tangents of angles are replaced by the angles themselves. Therefore, s should be long compared with d , and the value of r should be as close to 0.5 as practicable in order to prevent a coupling of gravity and torsional-pendulum effects.

K_i was determined by the equation

$$K_i = I\omega_i^2 \quad (7)$$

where ω_i is the wind-off frequency.

D_i was determined from the equation

$$D_i = 2I\left(\frac{D}{2I}\right)_i \quad (8)$$

~~CONFIDENTIAL~~

NACA RM L53H25

where $\left(\frac{D}{2I}\right)_1$ is the wind-off damping factor.

It might be mentioned here that the sequence of tests for each run was as follows: one wind-off test, two tests at one Reynolds number, two tests at the second Reynolds number, and a second wind-off test.

Since K_1 and D_1 were found to be essentially invariant with pressure from 1 to 0.1 atmospheres and there was no significant change in D_1 with amplitude, the K_1 and D_1 values used were the mean of all wind-off tests. In equation (5),

$$D_a = \frac{\partial M}{\partial \dot{\alpha}} + \frac{\partial M}{\partial q} \\ = \frac{1}{2} \rho V^2 S \bar{c} \frac{\partial C_m}{\partial \dot{\alpha}} + \frac{1}{2} \rho V^2 S \bar{c} \frac{\partial C_m}{\partial q} \quad (9)$$

Inasmuch as in stability notation C_{m_q} and $C_{m_{\dot{\alpha}}}$ are defined as $\frac{\partial C_m}{\partial \frac{q \bar{c}}{2V}}$

and $\frac{\partial C_m}{\partial \frac{\dot{\alpha} \bar{c}}{2V}}$, respectively,

$$C_{m_q} + C_{m_{\dot{\alpha}}} = \frac{4D_a}{\rho S V \bar{c}^2} \quad (10)$$

Similarly, since $C_{m_{\dot{\alpha}}} = \frac{\partial C_m}{\partial \dot{\alpha}}$

$$C_{m_{\dot{\alpha}}} = \frac{2K_a}{\rho S V^2 \bar{c}} \quad (11)$$

~~CONFIDENTIAL~~

CONFIDENTIAL

The value of K_a was determined by subtracting K_l from the total wind-on spring constant obtained from

$$\omega = \sqrt{\frac{K}{I} - \left(\frac{D}{2I}\right)^2}$$

Precision of Data

There are two main sources of error involved in this method, one source is directly associated with the flexural pivot and the other is inherent in the data reduction method.

With regard to the flexural pivot, it was originally intended to use several different flexure plates of varying thicknesses in order to attain a fairly wide range of frequencies for the damping tests. As the thickness of the plates increased, however, not only did K_l and D_l increase, they also became increasingly erratic. This condition was a direct result of size limitations. The dimensions of the flexural-pivot assembly (fig. 3) were such that 0-80 screws were the largest that could be used to hold the flexure plate rigidly against the flexure-plate base. This size was not sufficient to prevent some friction from taking place. To lessen this effect, only the thinnest flexure plates (0.008 inch thick) were used. The characteristics of these plates, as determined from all wind-off tests were:

$$\left(\frac{D}{2I}\right)_1 = 0.042 \pm 0.007$$

which was 11.2 percent of the smallest $\frac{D}{2I}$ value found from all wind-on tests, and

$$K_l = 0.186 \pm 0.002$$

which was 11.3 percent of the smallest K value for the test.

With regard to the errors involved in the data reduction, it is necessary to determine the distance from a point on a curve to the intersection of the tangent to the curve at that point with a straight line. As the angle between the tangent and the straight line decreases, the error involved in the graphical construction increases. Thus, the probable error involved varies with angle of attack, the error being least at the higher angles of attack and greatest at the lower angles of attack. In view of these conditions, it is difficult to determine some particular

number which would represent the overall precision of the data. Since the previously mentioned source of error probably overshadows all other probable errors it is believed that it should merely be pointed out that $C_{mq} + C_{m\alpha}$ is more accurate at the higher angles of attack than at the lower ones, and that any peculiar behavior of $C_{mq} + C_{m\alpha}$ at the low angles of attack should be viewed with suspicion.

For the sake of completeness, the following additional uncertainties are pointed out:

(a) Although, as indicated in reference 3, D_l may vary with frequency, no information on the possible variation of D_l with frequency was obtained for this series of tests.

(b) The value of D_l is determined under no-load conditions and this quantity is then subtracted from the total wind-on damping when the spring mechanism is subjected to oscillating lift and drag forces. It is believed that the number used to represent D_l is at least of the correct order of magnitude; however, actual load conditions were not simulated.

(c) The support wire, although under 250 pounds of tension, is nonetheless flexible and therefore subject to deflection under load. Estimates of the drag of the 30° delta-wing-body combination at $R = 1.69 \times 10^6$ give a zero lift drag of about 5 pounds plus an oscillating drag force of from 0 to 1 pound for a range of amplitude of 0° to 5° . A dead weight of 5 pounds suspended from the center of the support wire gave a deflection in the wire of 0.052 inch. Assuming a linear displacement with load, as the model oscillates, the center of the wire will move rearward periodically a maximum of about 0.01 inch. It may therefore be said that the center of rotation is known to within less than 0.01 inch, this amount decreasing as the amplitude decreases.

RESULTS

Test results on the 45° wing were irreducible and hence are not presented. There are two related reasons for this irreducibility.

The first reason is associated with the airfoil shapes of this series of tests, which were flat plates with beveled edges. A simple two-dimensional analysis shows that this type of section, if there is any tendency toward flow separation, has two positions of zero lift, $\pm\alpha$, where α is a function of the pressure-distribution change associated

with the separation. Figure 6 shows part of the oscillation record for the 45° wing at $M = 1.93$ and $R = 0.54 \times 10^6$ from which it can be seen that, although the wing initially oscillated about 0° angle of attack, after a few cycles it suddenly began to oscillate about some angle of attack other than zero.

The second reason is that for the 45° wing $\frac{c_0}{c} = 0.94$; that is, the point of rotation is located at $0.04c$ ahead of the theoretical center of pressure for a flat plate. With such a small moment arm, the effect of any shift of the center of pressure will be greatly magnified and will show up as a variation in frequency, which is a measure of $K_l + K_a$. Figure 7 is a plot of frequency in cycles per second against time, as taken from figure 6. Superimposed on this plot is the natural frequency of the model with the wind off. The difference between these two curves is a measure of $C_{m\alpha}$. It can be seen that while the model was oscillating about 0° angle of attack, $C_{m\alpha}$ decreased with time from positive to negative values; that is, as α decreased, the center of pressure moved from behind to ahead of the point of rotation. Then, when the mean oscillation angle changed from zero to its new value, $C_{m\alpha}$ became discontinuously positive and increased with time, or there was a discontinuous rearward shift in the center of pressure, after which it continued to move rearward. Thus, the separation coupled with the small moment arm of the 45° wing combined to make the data irreducible. For the tests of the 45° wing at higher Reynolds numbers the effects mentioned here were less pronounced, but the tendencies were the same.

Although the same wing section was used for the other wings of the investigation, it is believed that the separation tendency noted on the 45° wing did not interfere with data reduction for the other wings because for the 25° , 30° , and 35° wings the mean oscillation angle did not change from 0° .

Figures 8, 9, and 10 present the variation of $C_{m_q} + C_{m\dot{\alpha}}$ with amplitude for the wings of 25° , 30° , and 35° semiapex angles, respectively. Figures 11 to 13 present the corresponding plots of $C_{m\alpha}$ against amplitude.

The solid lines on figures 8 to 10 represent the theory of reference 4, whereas, the solid lines on figures 11 to 13 represent the theoretical prediction obtained by combining the method of reference 4 with that of reference 5.

Each plot of $C_{m_q} + C_{m\dot{\alpha}}$, with the exception of figure 10(b), has at least four sets of points representing two or more different tests. For

each test the unflagged symbols represent values obtained from the top oscillation curve and the flagged symbols represent values from the bottom curve. Where an unflagged symbol occurs without a corresponding flagged one, the two points coincided.

Figures 8(a) and 9(a) contain more sets of points than the other figures because some unusual results of the original data were questioned. Additional tests at a higher initial amplitude than originally employed were made which showed that in a certain frequency range and above an amplitude of about 1.5° the support system interfered with the model. This interference was evidenced by the appearance of beats in the oscillation record in the higher amplitude range. The beats were a clear indication that some external source was feeding periodic pulses of energy back into the system. This source could only be the support system. Figures 8(a) and 9(a), at the lowest Reynolds number, fell within this frequency range. Therefore data above about $\alpha_0 = 1.5^\circ$ are not presented for these figures.

On the left-hand side of figure 8(a) are presented four sets of data; three sets at $R = 1.31 \times 10^6$ and one at $R = 1.67 \times 10^6$. Increasing R by 27 percent produced a noticeable change in the damping in the higher amplitude range and caused a greater variation of damping with amplitude. The three sets of data on the right-hand side of figure 8(a) check fairly well except in the very low amplitude range, where, as previously pointed out, the accuracy is doubtful.

The data of figures 8(c) and 11(c) are questionable. During the test at $R = 0.96 \times 10^6$ the model was fluttering slightly in yaw. As the Reynolds number was decreased both the yawing amplitude and frequency increased. At $R = 1.04 \times 10^6$ the flutter ceased abruptly. The next two tests were made at a nominal Reynolds number of 1.09×10^6 ; the first of these tests (diamond-shaped symbol) was actually at $R = 1.07 \times 10^6$ and the second (triangular symbol), at 1.10×10^6 . It is difficult to conceive of such a small change in Reynolds number causing such a large difference in the two curves shown. Although these two tests were made close to the yaw stability boundary, the fact that the lower Reynolds number test, which was in the flutter-in-yaw regime, did not exhibit any drastic changes in damping suggests that the changes noted are not due to any possible coupling of lateral and longitudinal effects.

This particular test took place in about the middle of the series and inasmuch as all succeeding tests were satisfactory, equipment trouble is eliminated. Since the wing leading edge in this case was transonic ($\beta \tan \epsilon = 1.024$), figure 8(c) may be an indication that when the Mach lines are close to the leading edge, a random variation of the damping can be expected.

Figure 9(a) on the left consists of three sets of data; two at $R = 1.17 \times 10^6$, one with and one without transition strip, and one at $R = 1.69 \times 10^6$ without transition strip. In the upper amplitude region at $R = 1.69 \times 10^6$, the damping is slightly lower than for the other two tests, increasing with decreasing amplitude until it joins, and thereafter follows, the test at $R = 1.17 \times 10^6$ with transition strip. The damping for $R = 1.17 \times 10^6$ without transition strip develops a hump in the vicinity of $\alpha_0 = 0.75^\circ$. Inasmuch as this hump approaches the level of the damping for $R = 0.75 \times 10^6$ (on the right-hand side of figure 8(a)) without transition strip, it would appear that the hump is caused by separation effects in the lower amplitude range. It is noteworthy that the test at $R = 0.75 \times 10^6$ with transition strip gives a damping which is of the same order of magnitude as that for the higher Reynolds number tests.

A general examination of figures 8 to 10 indicates that within the range of these tests, $C_{m_q} + C_{m_a}$ may be satisfactorily approximated by theory. In some cases, the experimental results indicate a slight variation of $C_{m_q} + C_{m_a}$ with amplitude. This variation, when it occurs, is generally one of increasing damping with decreasing amplitude.

From figures 11 to 13 it can be seen that the accuracy of the theoretical prediction of C_{m_a} increases as $\beta \tan \epsilon$ increases until, when the leading edge is well supersonic, the agreement between theory and experiment is excellent.

CONCLUDING REMARKS

An investigation has been conducted at Mach numbers of 1.62, 1.93, and 2.41 to determine the damping in pitch of four delta-wing and body combinations for a Reynolds number range of 0.44×10^6 to 1.69×10^6 based on the mean aerodynamic chord of the wings. The semiapex angles of the wings were 25° , 30° , 35° , and 45° . The results are presented as a function of amplitude. Within the scope of these tests the following conclusions are indicated:

~~CONFIDENTIAL~~

NACA RM L53H25

The damping-in-pitch parameter $C_{mq} + C_{md}$ may be satisfactorily approximated by the theory.

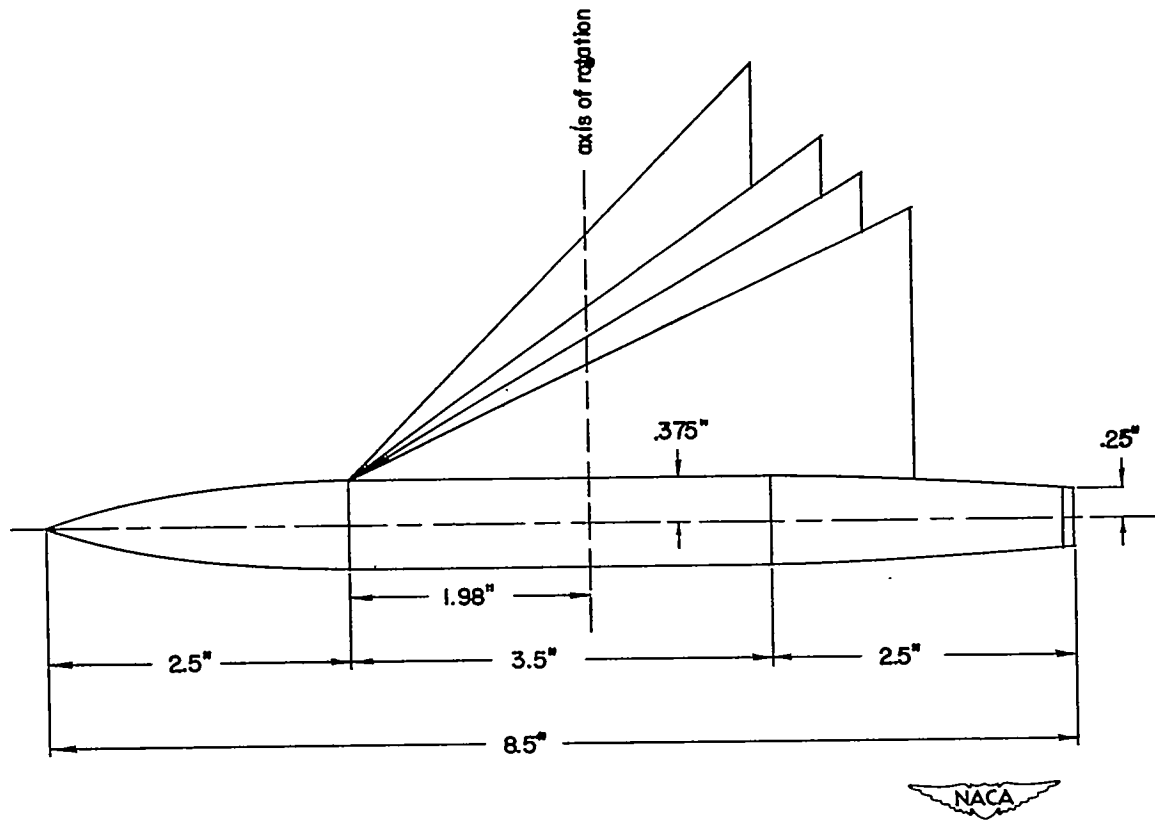
Where a variation of $C_{mq} + C_{md}$ with amplitude occurs, it is usually small and the damping increases with decreasing amplitude.

Langley Aeronautical Laboratory,
National Advisory Committee for Aeronautics,
Langley Field, Va., August 18, 1953.

REFERENCES

1. Tobak, Murray, Reese, David E., Jr., and Beam, Benjamin H.: Experimental Damping in Pitch of 45° Triangular Wings. NACA RM A50J26, 1950.
2. Tobak, Murray: Damping in Pitch of Low-Aspect-Ratio Wings at Subsonic and Supersonic Speeds. NACA RM A52L04a, 1953.
3. Beam, Benjamin H.: The Effects of Oscillation Amplitude and Frequency on the Experimental Damping in Pitch of a Triangular Wing Having an Aspect Ratio of 4. NACA RM A52G07, 1952.
4. Henderson, Arthur, Jr.: Pitching-Moment Derivatives C_{mq} and C_{md} at Supersonic Speeds for a Slender-Delta-Wing and Slender-Body Combination and Approximate Solutions for Broad-Delta-Wing and Slender-Body Combinations. NACA TN 2553, 1951.
5. Spreiter, John R.: Aerodynamic Properties of Slender Wing-Body Combinations at Subsonic, Transonic, and Supersonic Speeds. NACA TN 1662, 1948.

~~CONFIDENTIAL~~

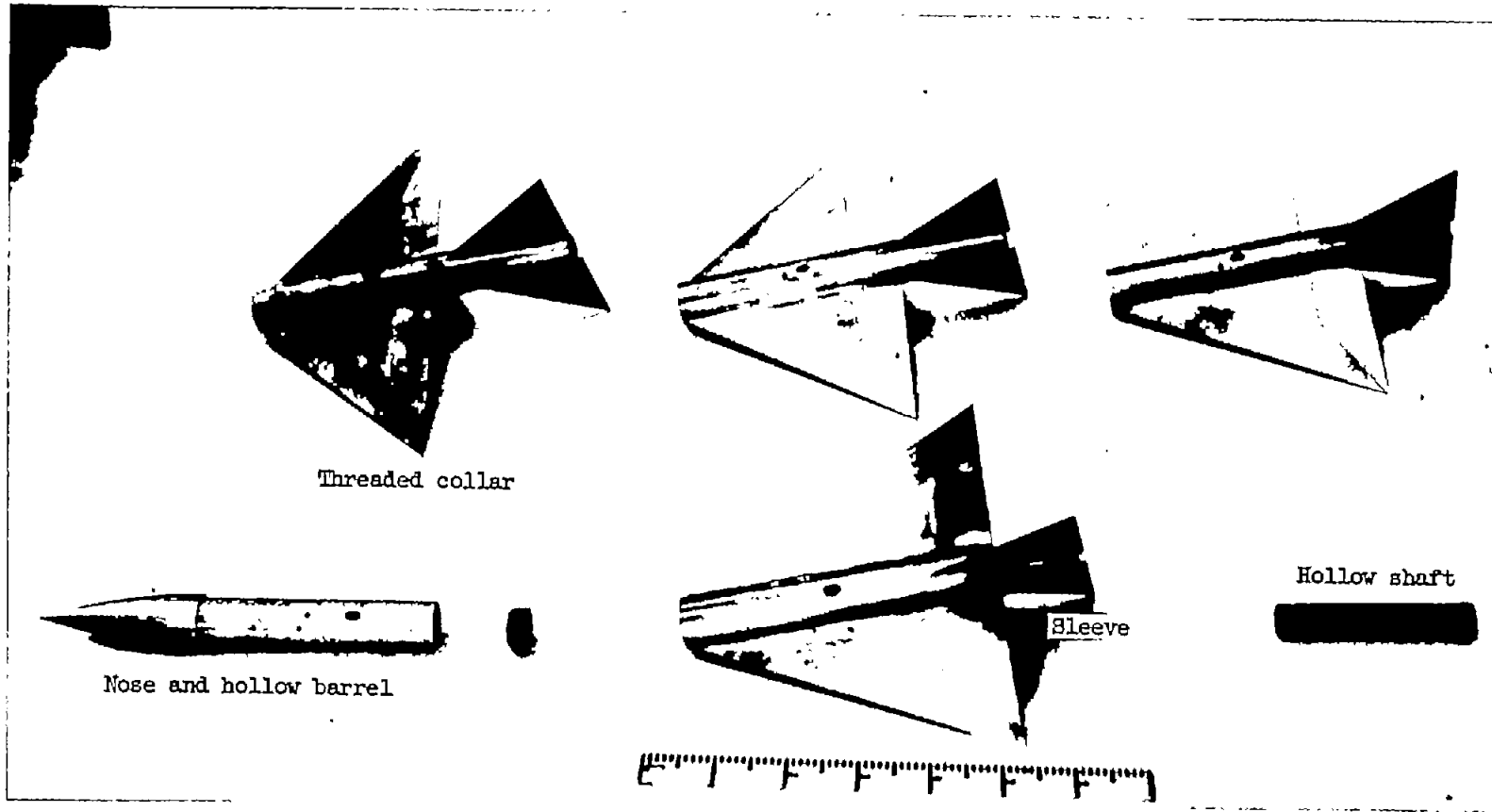


ϵ	$\frac{a}{s}$	S	\bar{c}	c_0
25°	.147	14"	3.65"	2.78"
30°	.132	14"	3.28"	2.63"
35°	.120	14"	2.98"	2.52"
45°	.100	14"	2.50"	2.36"

(a) Wings and body of test models.

Figure 1.- Test models.

CONFIDENTIAL



(b) Component parts of models.

L-80292

Figure 1.- Concluded.

NACA RM 153H25

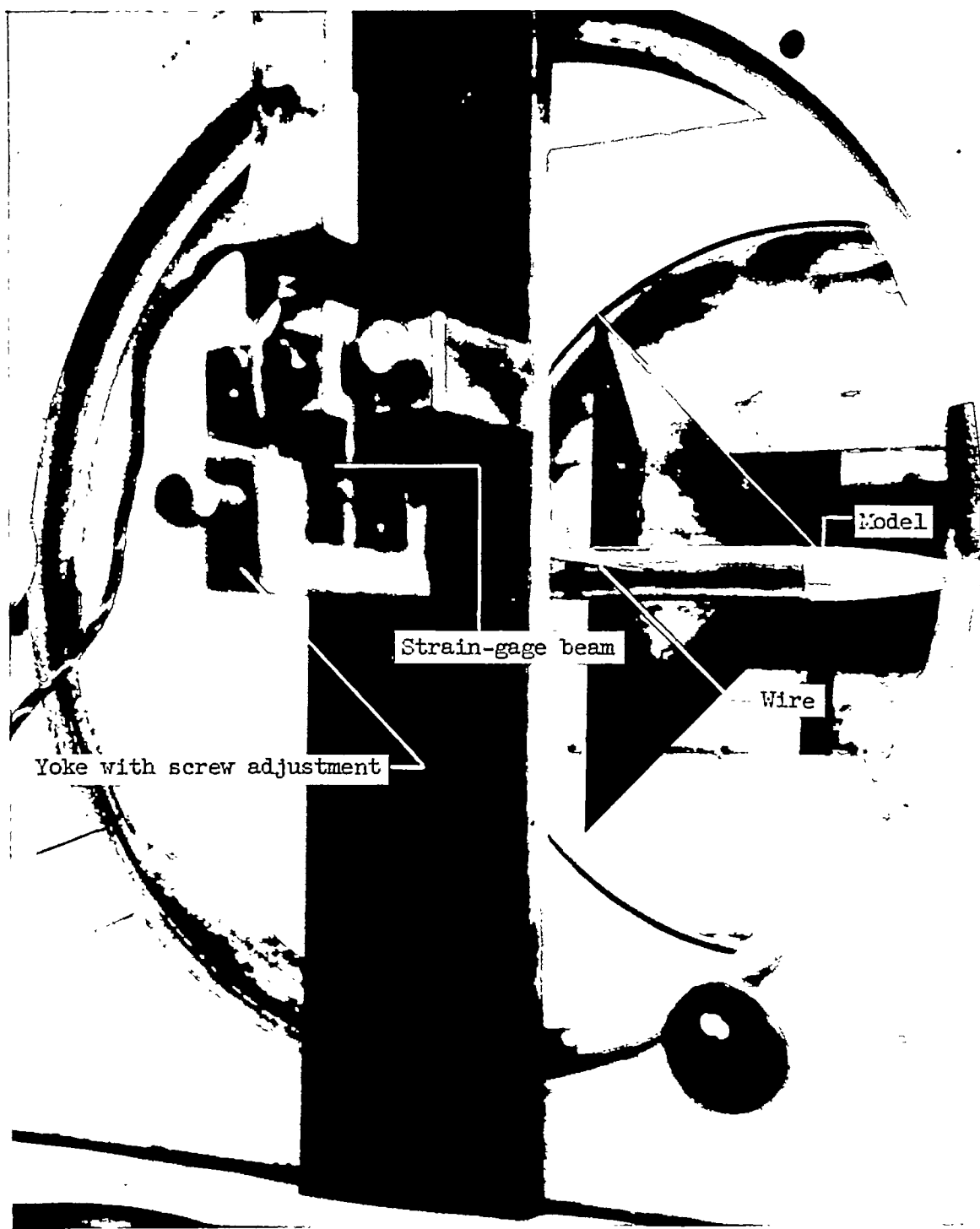


Figure 2.- Model mounted in a mock-up of the test section.

L-80293

~~CONFIDENTIAL~~

NACA RM L53H25

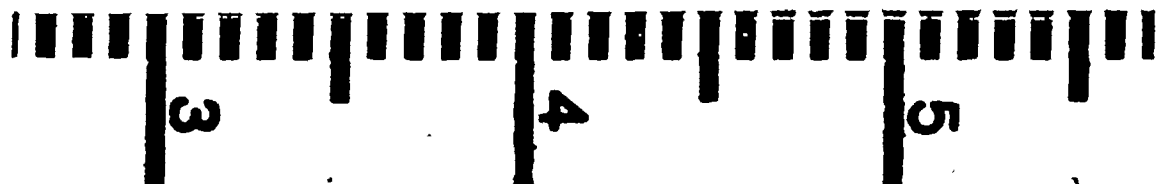
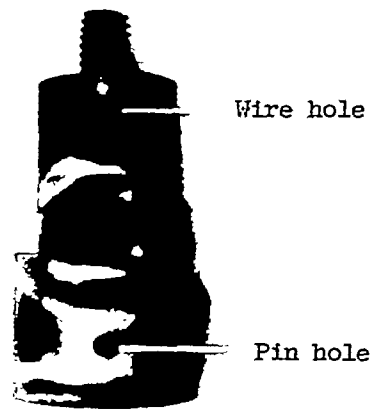


Figure 3.- Two views of flexural-pivot assembly.

L-80294

~~CONFIDENTIAL~~



L-80295

Figure 4.- Typical oscillation record; $\epsilon = 25^\circ$; $M = 1.62$; $R = 1.31 \times 10^6$;
initial $\alpha_0 = 2.70^\circ$.

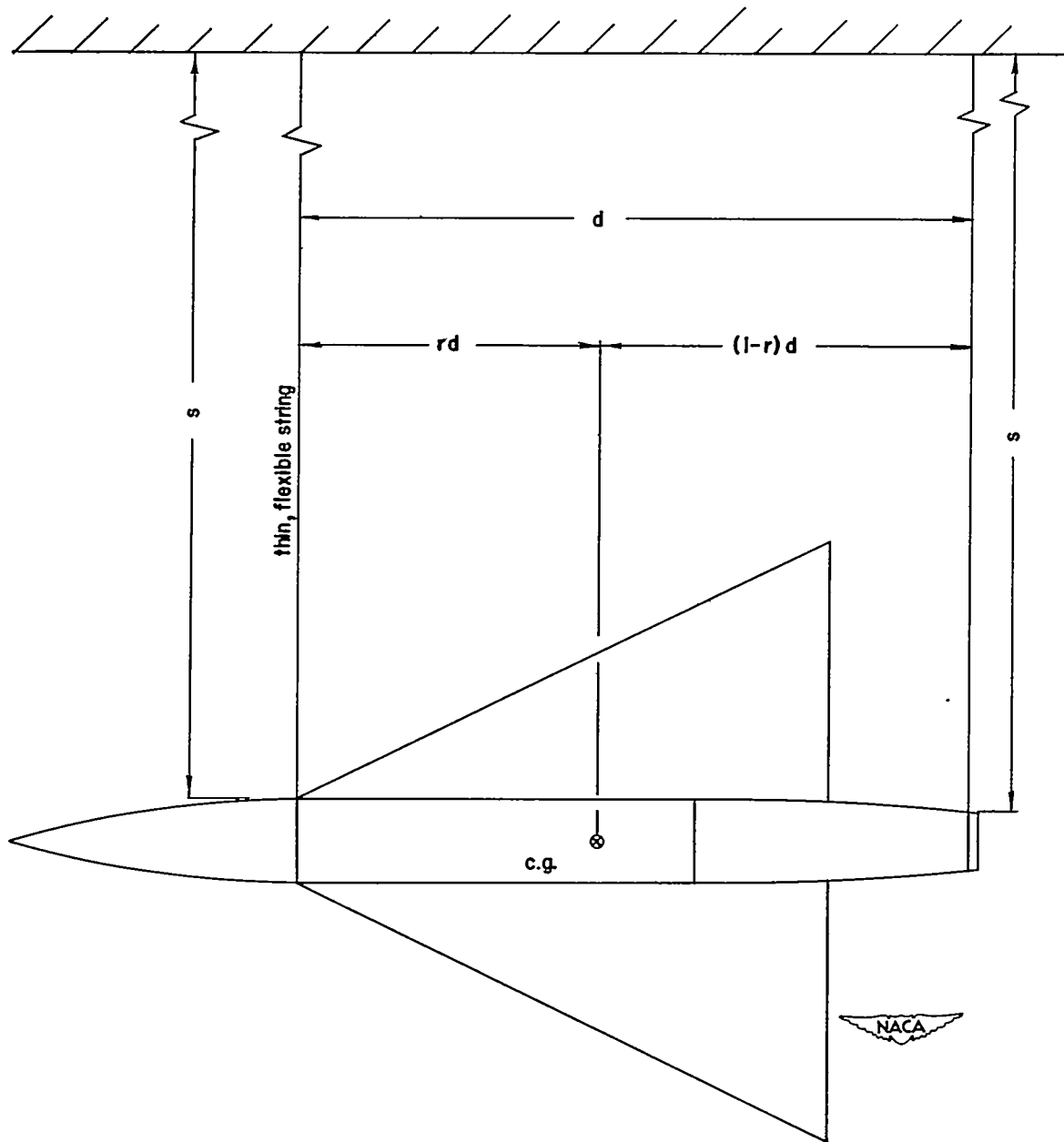
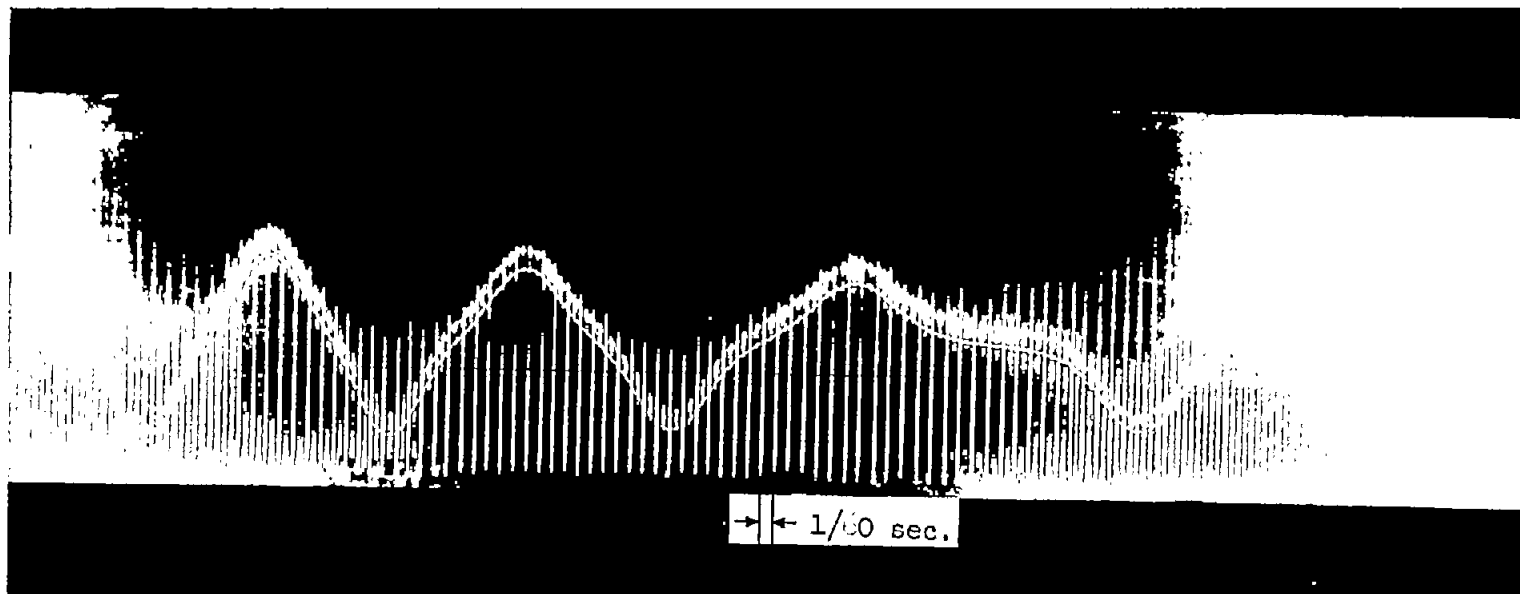


Figure 5.- Bifilar pendulum setup.

CONFIDENTIAL

CONFIDENTIAL



L-80296
Figure 6.- Section of oscillation record for $\epsilon = 45^\circ$; $M = 1.93$;
 $R = 0.54 \times 10^6$.

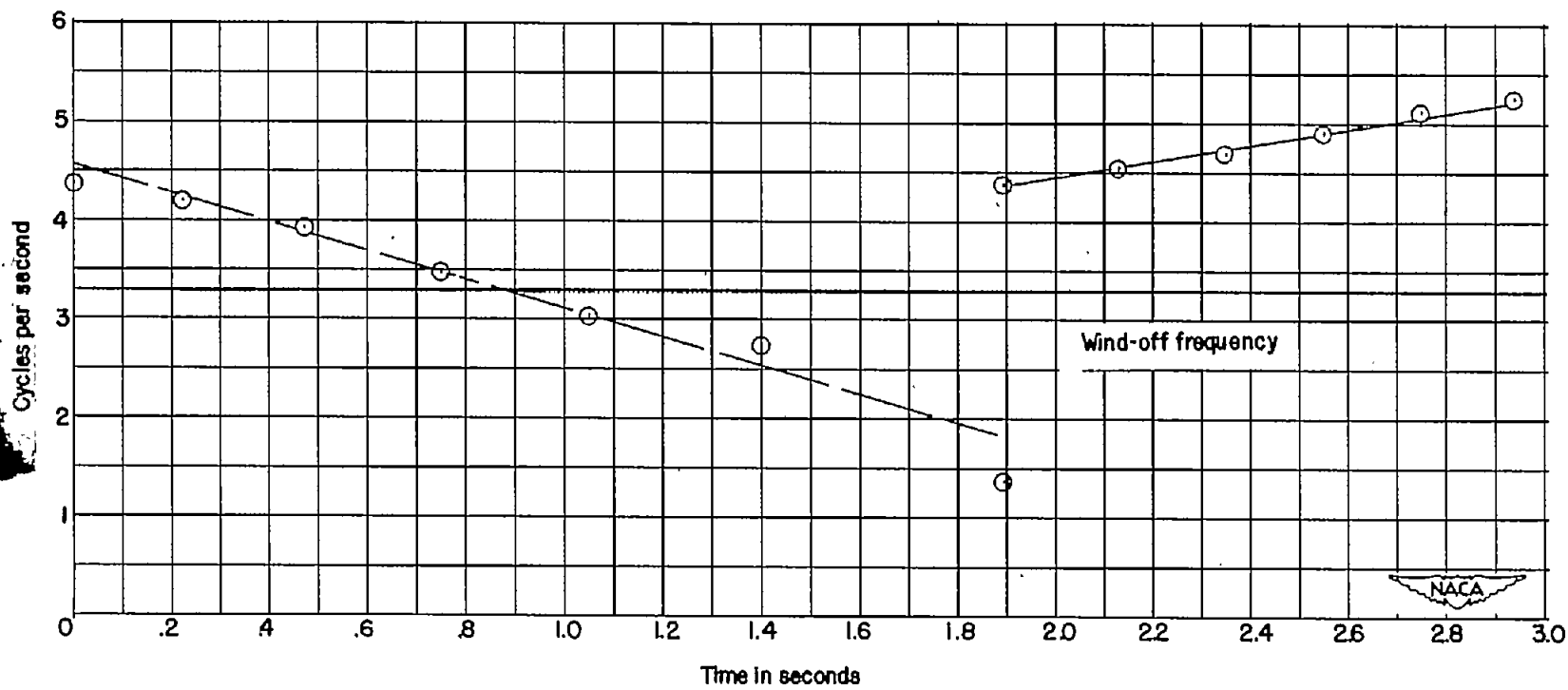


Figure 7.- Variation of frequency with time for 45° wing. $M = 1.93$;
 $R = 0.54 \times 10^6$.

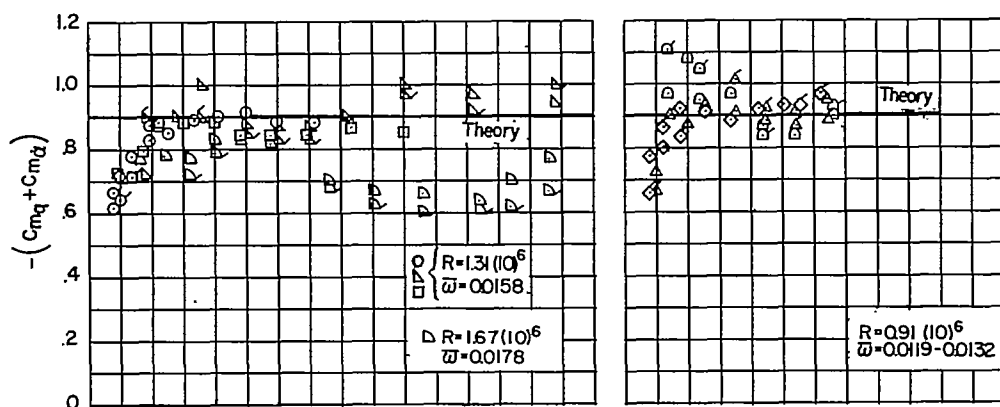
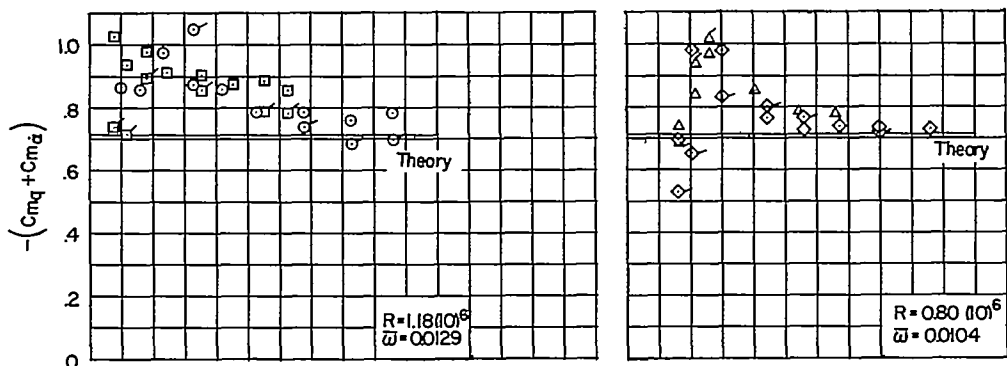
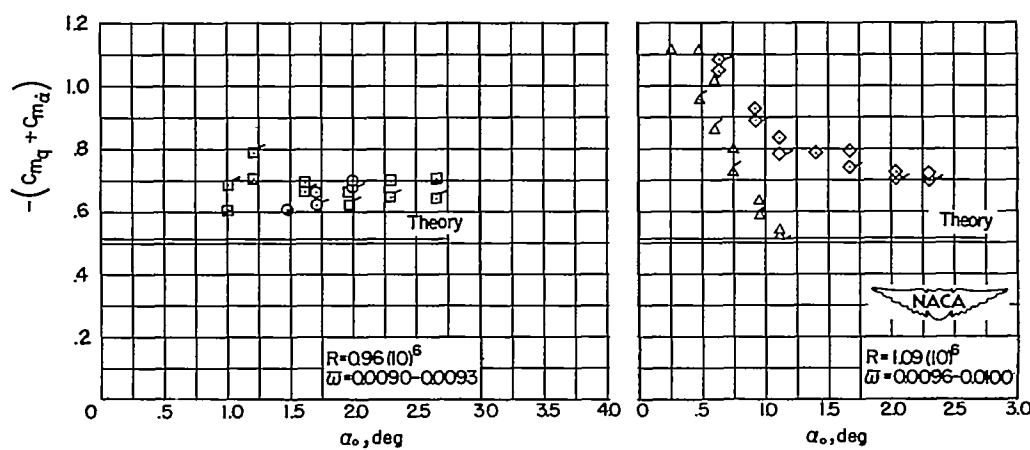
(a) $M = 1.62; \beta \tan \epsilon = 0.594$.(b) $M = 1.93; \beta \tan \epsilon = 0.770$.(c) $M = 2.41; \beta \tan \epsilon = 1.024$.

Figure 8.- Variation of $C_{m_q} + C_{m_a}$ with amplitude for $\epsilon = 25^\circ$; $\frac{c_o}{c} = 0.76$.

(Flagged symbols refer to bottom oscillation curve.)

CONFIDENTIAL

NACA RM L53H25

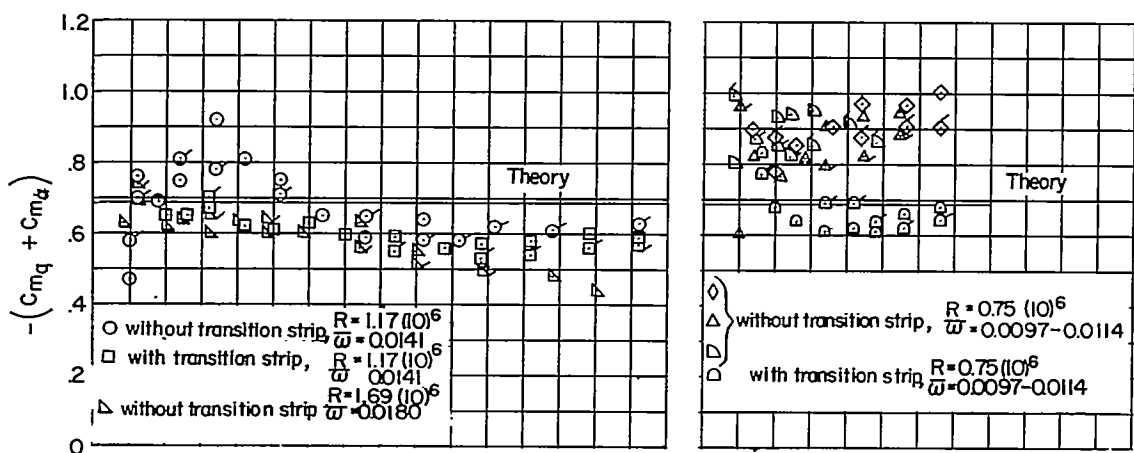
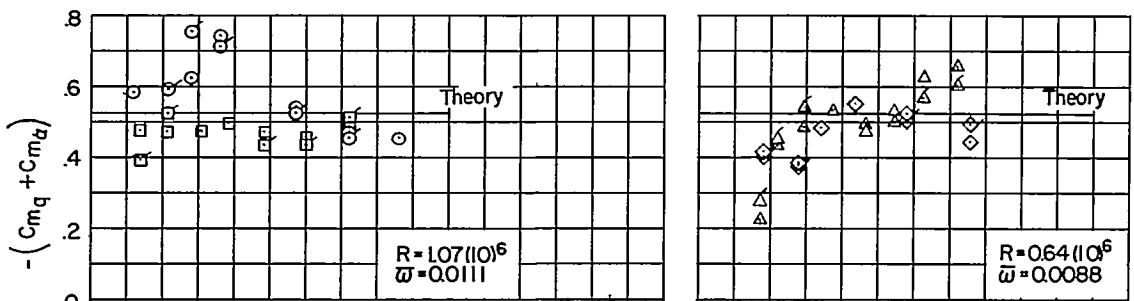
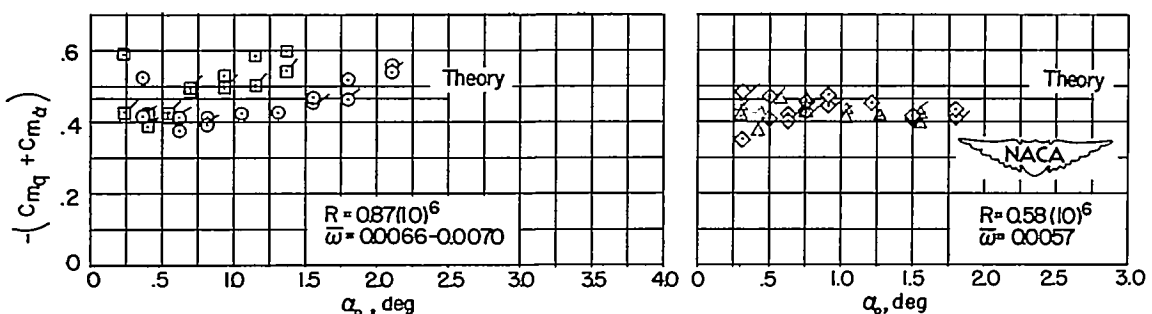
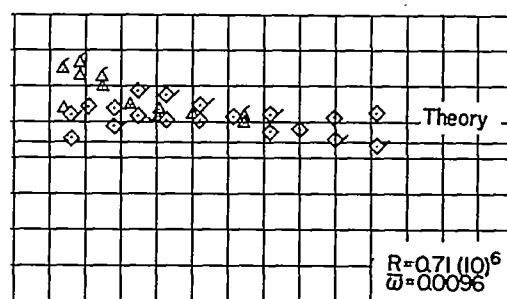
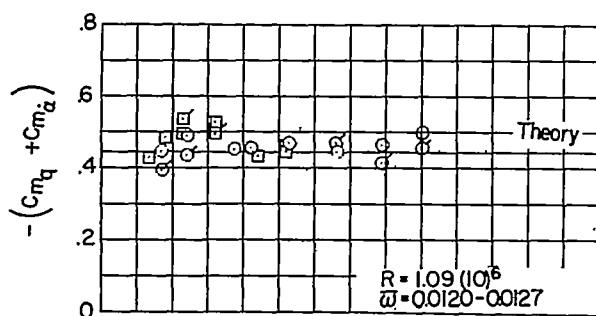
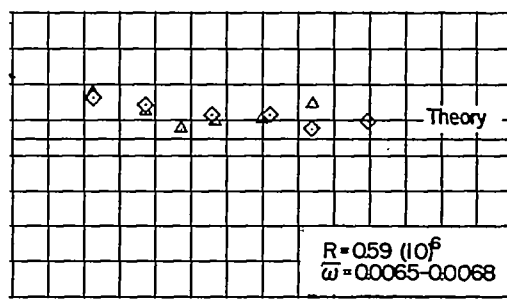
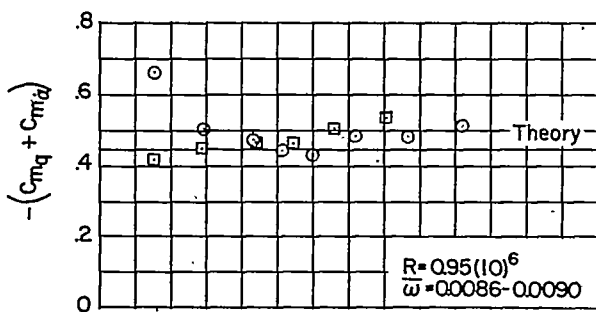
(a) $M = 1.62$; $\beta \tan \epsilon = 0.736$.(b) $M = 1.93$; $\beta \tan \epsilon = 0.953$.(c) $M = 2.41$; $\beta \tan \epsilon = 1.266$.

Figure 9.- Variation of $C_{m_q} + C_{m_\alpha}$ with amplitude for $\epsilon = 30^\circ$; $\frac{c_o}{c} = 0.80$.

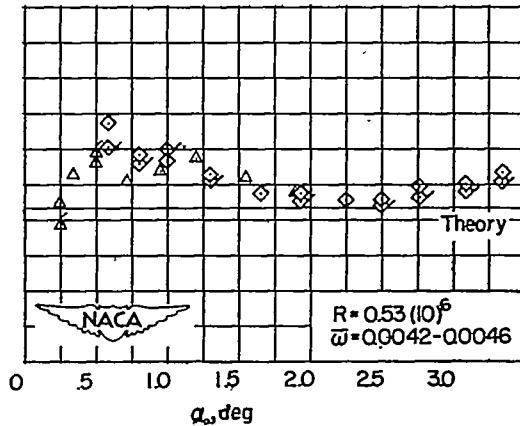
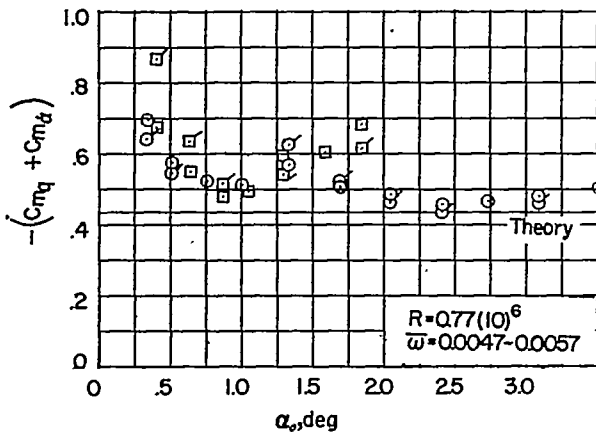
(Flagged symbols refer to bottom oscillation curve.)



(a) $M = 1.62; \beta \tan \epsilon = 0.893.$



(b) $M = 1.93; \beta \tan \epsilon = 1.155.$

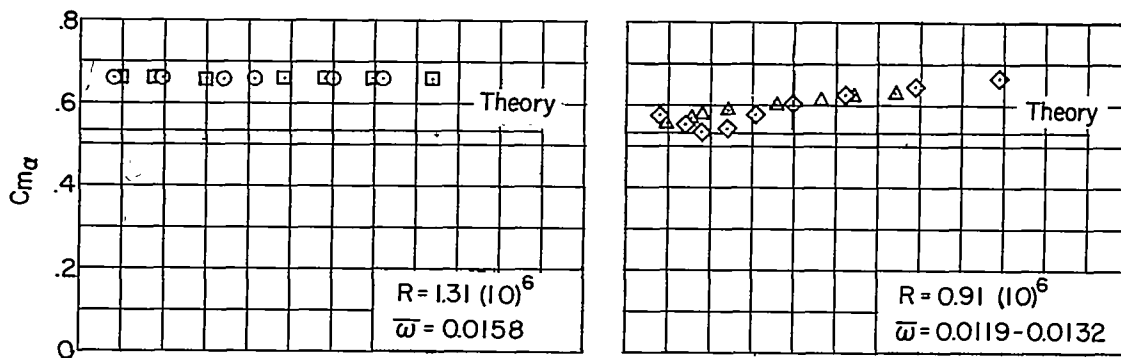
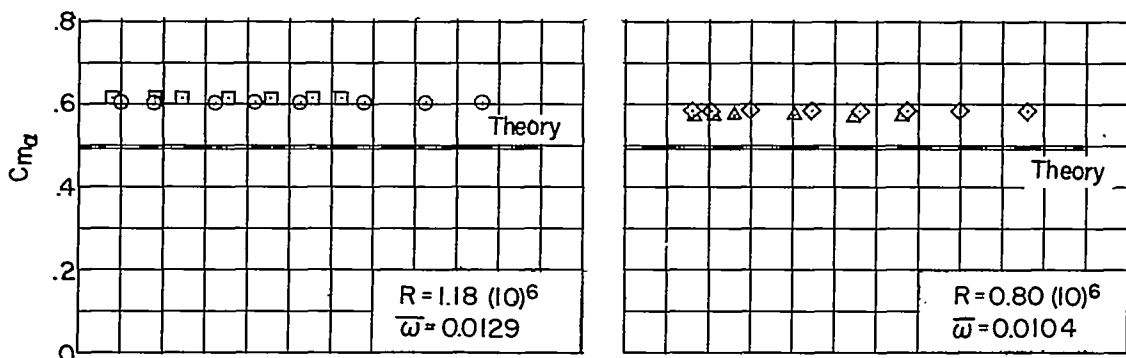
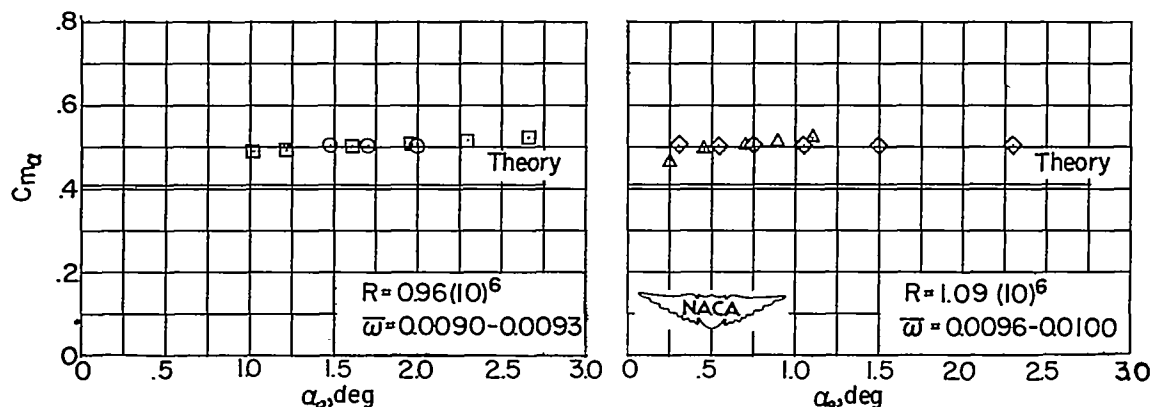


(c) $M = 2.41; \beta \tan \epsilon = 1.536.$

Figure 10.- Variation of $C_{m_q} + C_{m_d}$ with amplitude for $\epsilon = 35^\circ$; $\frac{c_o}{c} = 0.85$.

(Flagged symbols refer to bottom oscillation curve.)

CONFIDENTIAL

(a) $M = 1.62; \beta \tan \epsilon = 0.594$.(b) $M = 1.93; \beta \tan \epsilon = 0.770$.Figure 11.- Variation of $C_{m\alpha}$ with amplitude for $\epsilon = 25^\circ$; $\frac{C_0}{C} = 0.76$.

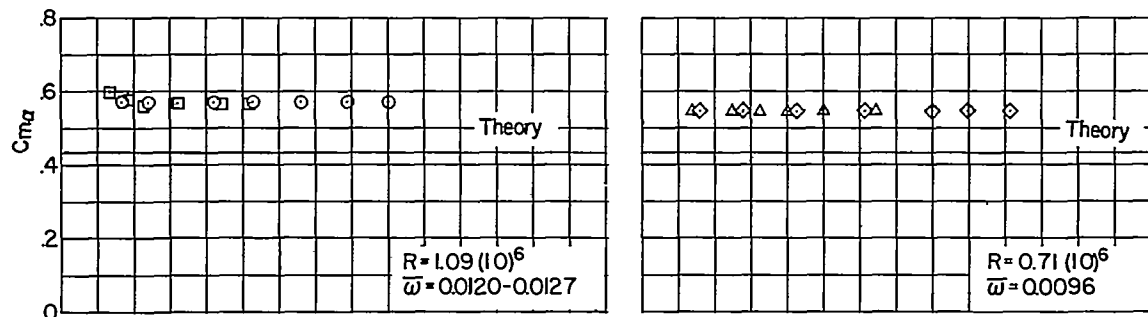
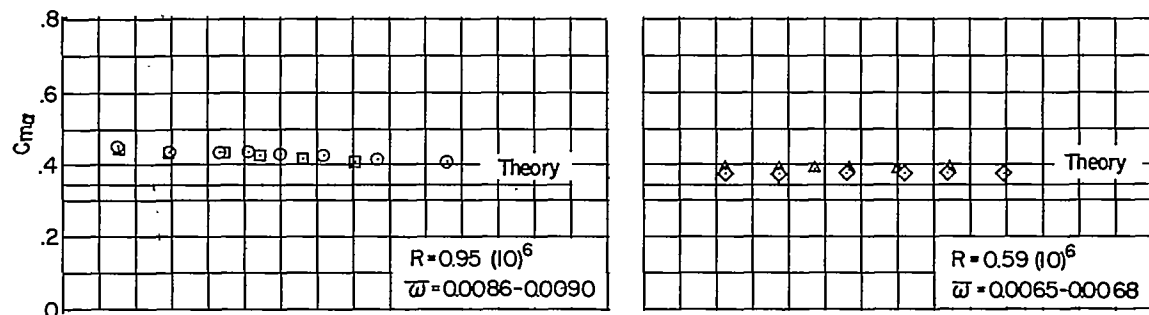
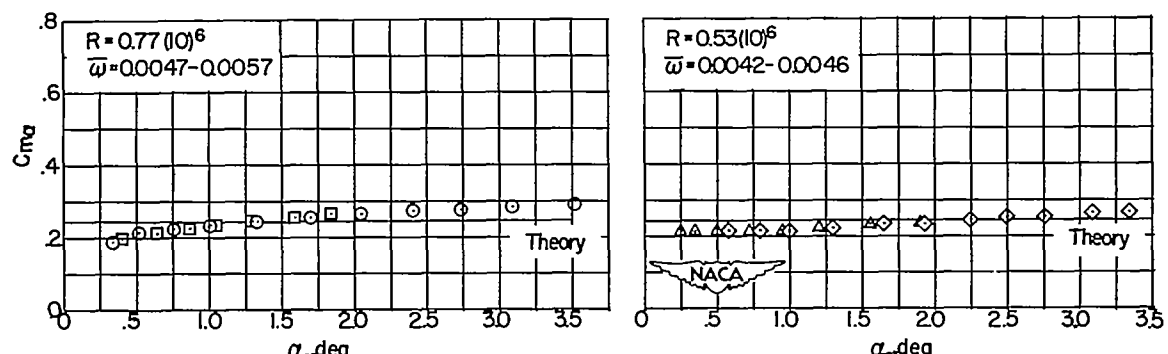
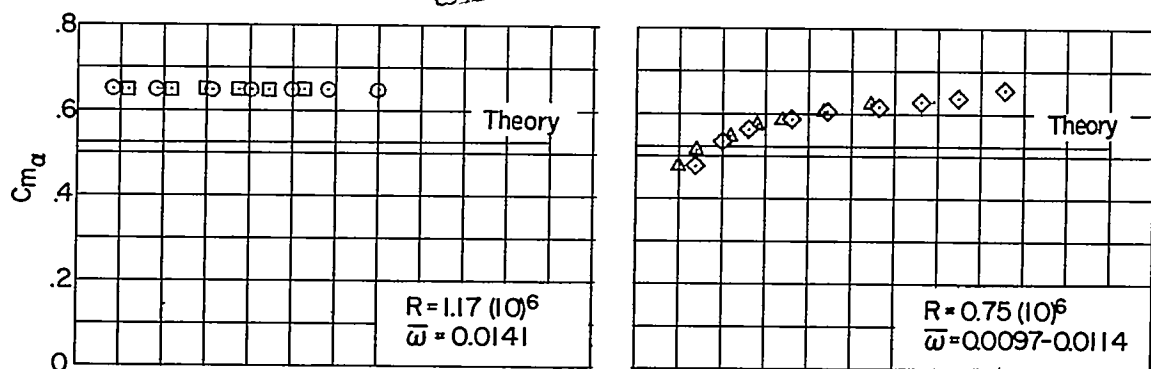
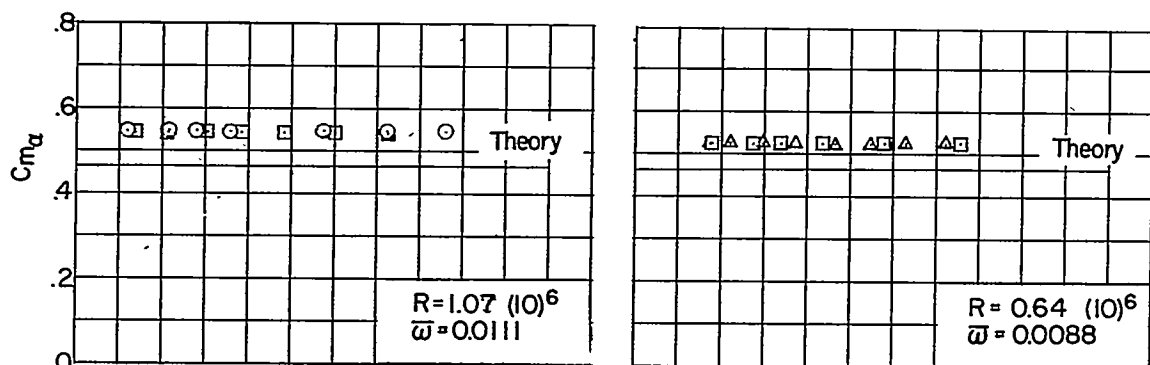
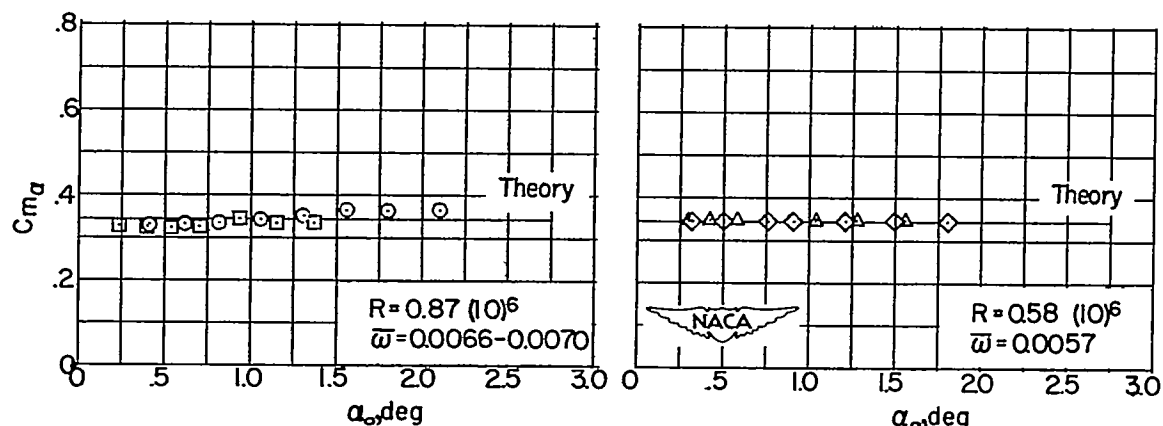
(a) $M = 1.62; \beta \tan \epsilon = 0.893.$ (b) $M = 1.93; \beta \tan \epsilon = 1.155.$ (c) $M = 2.41; \beta \tan \epsilon = 1.536.$

Figure 13.- Variation of $C_{m\alpha}$ with amplitude for $\epsilon = 35^\circ$; $\frac{c_o}{c} = 0.85$.

(a) $M = 1.62; \beta \tan \epsilon = 0.736.$ (b) $M = 1.93; \beta \tan \epsilon = 0.953.$ (c) $M = 2.41; \beta \tan \epsilon = 1.266.$ Figure 12.- Variation of $C_{m\alpha}$ with amplitude for $\epsilon = 30^\circ$; $\frac{c_0}{c} = 0.80$.